IC/71/136

TOPICAL SEMINAR
ON ELECTROMAGNETIC INTERACTIONS
ICTP, Trieste, 21-26 June 1971.

International Atomic Energy Agency
and
United Nations Educational Scientific and Cultural Organization
INTERNATIONAL CENTRE FOR THEORETICAL PHYSICS

DEEP INELASTIC ELECTRON SCATTERING: EXPERIMENTAL *

Jerome I. Friedman

Department of Physics
and
Laboratory for Nuclear Science**
Massachusetts Institute of Technology, Cambridge, Mass., USA.

MIRAMARE - TRIESTE
October 1971

* An invited talk presented at the above seminar.

** Work supported in part through funds provided by the US Atomic Energy Commission under Contract No. AT(30-1)2098.

In this talk I want to review and bring up to date the experimental information on high energy inelastic electron scattering from the proton and neutron.

Inelastic electron nucleon scattering has been carried out at various accelerators for over a decade. With the advent of SLAC, the higher energies and intensities have made available a new region of inelastic scattering to be investigated, commonly referred to as the "deep inelastic" region, which corresponds to the excitation of the continuum well beyond the resonance region.

Since 1967 the SLAC-MIT Collaboration[1] has been carrying out a program of inelastic electron scattering in a singles experiment over a wide range of four momentum transfers and missing masses of the recoiling hadronic system. The reactions that have been studied are inelastic electron scattering from the proton, deuteron, and a number of different nuclei. Experimental work on inelastic electron scattering has also been carried out at DESY[2], and there has been a program[3] of inelastic muon scattering at SLAC.

This discussion will center primarily on the experimental measurements from the SLAC-MIT group. I will not say much about the extensive theory that has been generated by this subject, because this will be covered in a number of subsequent talks.

Before proceeding to the results, a brief description of the experimental method[4] is in order. A relatively monochromatic electron beam from the linear accelerator passed through a liquid hydrogen target and then through a series of beam monitors. The scattered electrons were momentum analysed by a magnetic spectrometer. In separate experiments the SLAC 20 GeV/c and 8 GeV/c spectrometers were used to cover different kinematic regions. Downstream

of the magnetic elements of the spectrometer were placed scintillation counter hodoscopes which registered the momentum and scattering angle of each scattered electron. Behind the hodoscopes there were particle identification counters which were employed to identify electrons amid a background of π^- mesons. These consisted of a Cerenkov counter, a total absorption counter for electromagnetic cascades, and a few counters used to sample early shower development in the total absorption ceunter.

The range of kinematics covered in the SLAC-MIT measurements is given in Table I. The range of missing mass covered was $M < W < 5.5$ GeV and the range of the square of the four momentum transfer q^2 was $0.3 < q^2 < 20$ $(GeVc/)^2$. The missing mass W is the invariant mass of the unobserved final hadronic state and is given by

$$W^2 = 2M(E-E') + M^2 - q^2$$

where E is the incident electron energy, E' is the scattered electron energy, and M is the mass of the target nucleon. The quantity q^2 is given by

$q^2 = 2EE'(1 - \cos\theta)$ where θ is the electron scattering angle.

In general, the measurements were made at closely spaced values of the scattered energy E' for constant scattering angle θ and constant incident energy E. For each scattering angle spectra were measured at a number of incident energies in order to be able to make model independent radiative corrections to the data.

I will first discuss the inelastic electron-proton scattering results. Some typical spectra are shown in Figures 1 and 2. Bumps in the spectra are seen at the Δ1236, the N*1518, and in the region of the N*1688; and in a number of spectra there is a small bump near the Δ1920. No clear-cut evidence is seen for the excitation of the Roper P_{11} resonance. Unfortunately, I will not have time in this talk to discuss in detail the

behavior of the resonances excited in electron scattering. In addition to these bumps there is a broad continuum of large cross-section. These spectra have a qualitative similarity to those observed in inelastic electron-nuclear scattering. The spectra shown have full radiative corrections. While the radiative corrections are the largest corrections to the data and involve a considerable amount of computation, they are understood to within the 5% to 10% level and do not significantly increase the total error in the measurements. In Figure 3 is shown the relative magnitude of the radiative correction as a function of W for a typical spectrum.

The general behavior of the measured spectra as a function of laboratory energy and angle can be seen in Figures 4 and 5, in which some of the measured spectra are sketched.[5] These figures show that the excitation of discrete states is dominant for lower angles and incident energies, but at larger angles and incident energies the continuum channels dominate the scattering. The Mott cross-section (without the kinematic correction for target recoil) is given for each energy and angle to serve as a scale for the scattering cross-sections. The figures indicate that the resonances damp out more rapidly than the bulk of the continuum with increasing values of q^2.

To extract the effects of the nucleon structure in the scattering process it is useful to separate out the pure Q.E.D. dependence of the scattering cross-section. On the assumption of one photon exchange, the differential cross-section[6] in the laboratory frame for electron scattering in which only the scattered electron is detected is

$$\frac{d^2\sigma}{d\Omega dE} = \frac{e^4}{4E^2} \quad \frac{\cos^2\theta/2}{\sin^4\theta/2} \quad \left[W_2 + 2W_1 \tan^2 \theta/2 \right]$$

The structure functions W_1 and W_2 depend on the properties of the target nucleon and can be represented as functions of two invariants, q^2 and $\nu = E-E'$, the electron energy loss. The above expression is the analogue of the Rosenbluth cross-section. There is another expression[7] that is often used to describe inelastic electron scattering which is the analogue of photoproduction. In this description the cross-section for inelastic electron scattering is given by:

$$\frac{d^2\sigma}{d\Omega dE'} = \Gamma_t \left[\sigma_t(q^2, \nu) + \varepsilon\sigma_s(q^2,\nu)\right]$$

where σ_t and σ_s are the absorption cross-sections for virtual photons with transverse and longitudinal polarization components respectively,

$$\Gamma_t = \frac{\alpha}{4\pi^2} \frac{K}{q^2} \frac{E'}{E} \left(\frac{2}{1-\varepsilon}\right),$$

and

$$\varepsilon = \frac{1}{1 + 2(1 + \nu^2/q^2)\tan^2\theta/2} \; ; \; 0 \leq \varepsilon \leq 1$$

The quantity $K = (W^2 - M_p^2) / 2M_p$, where M_p is the rest mass of the proton. In the limit $q^2 \to 0$, $\sigma_s \to 0$, and $\sigma_t(q^2, \nu) \to \sigma_\gamma(\nu)$ where $\sigma_\gamma(\nu)$ is the photoabsorption cross-section for real photons of energy ν. The two descriptions are equivalent and it follows that

$$W_1 = \frac{K}{4\pi^2\alpha}\,\sigma_t$$

$$W_2 = \frac{K}{4\pi^2\alpha}\,\frac{q^2}{q^2+\nu^2}\,(\sigma_t + \sigma_s)$$

In order to make separate determinations of W_1 and W_2 (or σ_t and σ_s), it is necessary to measure the inelastic cross-section at different angles for the same values of q^2 and ν, requiring appropriate changes in the values of both E and E'.

The results of the separation are, for convenience, expressed in terms of the parameter $R = \sigma_s/\sigma_t$, and the experimental values of W_1 and W_2 are given by

$$W_1 = \left[\frac{d^2\sigma}{d\Omega dE'}\right]_{EXP} \left[\frac{d\sigma}{d\Omega_{Mott}}\right]^{-1} \left[(1+R)\,\frac{q^2}{q^2+\nu^2} + 2\tan^2\theta/2\right]^{-1}$$

$$W_2 = \left[\frac{d^2\sigma}{d\Omega dE'}\right]_{EXP} \left[\frac{d\sigma}{d\Omega_{Mott}}\right]^{-1} \left[1 + 2\left(\frac{1}{1+R}\right)\left(\frac{q^2+\nu^2}{q^2}\right)\tan^2\theta/2\right]^{-1}$$

where $\left[\frac{d^2\sigma}{d\Omega dE'}\right]_{EXP}$ is the experimental inelastic cross-section and $\frac{d\sigma}{d\Omega_{Mott}}$ is the Mott cross-section without recoil corrections.

Actual data points at different angles for the same values of q^2 and ν exist only for $q^2 = 4(GeV/c)^2$; W = 2,3, and 4 GeV, and for $q^2 = 1.89\ (GeV/c)^2$; W = 3 GeV. However, the data at each angle are sufficiently finely spaced that they can be reliably interpolated to a particular point in the q^2, ν plane. Separation with several different interpolation methods indicated that the results were relatively insensitive to the particular procedure used.

The assumption of one photon exchange which underlies the definition of the electron-magnetic structure functions, implies a linear dependence of $d^2\sigma/d\Omega dE'/\Gamma_t$ on ε for a particular point (q^2, ν). The data are everywhere consistent with this requirement. The values of R are in the range 0 to 0.5, and no striking kinematic variation is apparent. On the assumption that R is a constant in this kinematic range, the average value of R is 0.18 ± 0.10, where the quoted error includes an estimate of the systematic error. The values of R are also compatible with $R = aq^2$, with $a \simeq .035$ $(GeV/c)^{-2}$, and with $R \simeq q^2/\nu^2$. Various other forms would also be compatible with the results. In Figure 6 the measured values of R are shown as a function of q^2. This curve also gives the predictions of the ρ dominance model [8] of inelastic electron scattering which are seen to be incompatible with the data. The results of the separation show that σ_t is dominant in the kinematic region that was investigated, roughly given by $1.0 \leq q^2 \leq 11.0$ $(GeV/c)^2$ and $2.0 \leq W \leq 3.5 - 4.0$ GeV. The smallness of R precludes a definite statement that σ_s is significantly different from zero.

From the early measurements at 6° and 10°, combined with the assumption of a predominantly transverse electro-magnetic interaction, it was found that νW_2 depended only on the ratio of q^2 and ν over a substantial range of the data[9]. This property is referred to as "scaling" in the variable $\omega \equiv \frac{2M\nu}{q^2}$. On the basis of an investigation of models that satisfy current algebra, Bjorken[10] had predicted this behavior in the asymptotic kinematic region reached by letting ν and q^2 go to infinity with ω held constant. The large angle data have provided measurements at large values of q^2 and, in conjunction with the earlier measurements, information about R, allowing more stringent tests of scaling behavior to be made.

To test for scaling it is useful to plot νW_2 for fixed ω as a function of q^2. For constant ω scaling behavior is exhibited in such a plot if νW_2 is independent of q^2. Values of νW_2 for ω=4 are shown as a function of q^2 in Figure 7, calculated from interpolations of radiatively corrected spectra at 6^o, 10^o, 18^o, 26^o and 34^o. In Figure 8 experimental values of νW_2 are plotted as a function of q^2 for various ranges of ω. A constant value of R = 0.18 has been assumed in calculating νW_2. Scaling behavior is not expected where there are observable resonances because resonances occur at fixed W, not at fixed ω, nor is it expected for small q^2, because νW_2 cannot depend solely on ω in this limit. An inspection of a number of plots similar to these leads to a number of conclusions regarding the validity of scaling in several kinematic regions .

1. For $4 < \omega < 12$

For W > 2.0 GeV and $q^2 > 1.0$ GeV^2, νW_2 is a constant within experimental errors and hence "scales" in ω (or in any other variable). The range of kinematics for the measurements included in this test covers q^2 from 1 to 7 GeV^2 and values of W between 2 and 5 GeV.

2. For $\omega < 4$

The experimental values of νW_2 scale for W > 2.6 GeV, but νW_2 appears to increase as W decreases below 2.6 GeV. This region covers kinematic ranges of W between 2.6 GeV and 4.9 GeV, and of q^2 between 2 GeV^2 and 20 GeV^2.

3. For $\omega > 12$

There are relatively few points above q^2 = 1 GeV^2 and no points above q^2 = 2 GeV^2, making it difficult to determine any variation of νW_2 with changing q^2. There are no measurements of R in this region, and the values

of νW_2 are especially sensitive to variations in R. The large angle data have a maximum ω of 8 and influence the values of νW_2 for $\omega > 12$ only through the values of R determined in the low ω region. Scaling can not be tested critically in this region since the uncertainty in R prevents the large ω behavior of νW_2 from being known with assurance. If $R = 0.18$ is assumed, then for $q^2 > 0.8$ GeV^2, νW_2 decreases slightly as ω increases. However, for larger values of R, consistent with the extrapolated values, νW_2 is constant. Preliminary analysis of more recent data does not resolve these questions[11]. A falling νW_2 with increasing ω would indicate a non-diffractive component of W_2 at large ω.

The above conclusions rely on some extrapolation of the measured values of R over parts of the total kinematic region discussed. In order to test the sensitivity of the determinations of νW_2 to the different methods of extrapolation, the three forms consistent with the data were employed, namely, $R = 0.18$, $R = 0.031\ q^2/M_p$, and $R = q^2/\nu^2$. The conclusions regarding scaling behavior do not depend on the form used.

One of the most remarkable aspects of the above results is that the scaling behavior, presumed to be an asymptotic property, sets in as such low values of q^2 and ν. The theoretical significance of this is presently not understood. The question naturally arises as to whether there are other variables that converge to ω in the Bjorken limit and that provide scaling behavior at even smaller values of q^2 and ν. A number of such variables have been proposed. Among these are the variables proposed by suri[12], $\omega_s = s/q^2$; by Rubinstein and Rittenberg[13], $\omega_r = \left[2M\nu + M^2\right]/\left[q^2 + A^2\right]$; and by the SLAC-MIT group[14], $\omega' = \left[2M\nu + a^2\right]/q^2$. I do not have detailed studies of the variables ω_s and ω_r. The SLAC-MIT Variable, ω', has been found to extend

the scaling region from $W \simeq 2.6$ GeV down to $W \simeq 1.8$ GeV for the whole range of ω. The constant $\underline{a}$ was determined to be 0.95 ± 0.07 GeV^2 by fitting the data with $W > 1.8$ GeV and $q^2 > 1(\text{GeV/c})^2$. The statistical significance of $\underline{a}$ is greatly reduced in a fit to the data for $W > 2.6$ GeV implying that functions of either ω or ω' give satisfactory statistical fits in this kinematic range. In the following discussion, the value of $\underline{a}$ will be chosen to be equal to $M^2 = 0.88$ which gives $\omega' = \omega + M_p^2/q^2 = 1 + W^2/q^2$.

Figure 9 shows $2M_pW_1$ and νW_2 as functions of ω for $W \geq 2.6$ GeV, and Figure 10 shows these quantities as functions of ω' for $W \geq 1.8$ GeV. The data presented in both figures are for $q^2 > 1(\text{GeV/c})^2$ and use $R = 0.18$. The observed scaling behavior in ω and ω' is impressive for both structure functions over a large kinematic region. Such scaling behavior arises naturally in parton models[15,16,17] in which the electron scatters incoherently from pointlike constituents of the proton. Another theoretical approach[18] relates the inelastic scattering to virtual Compton scattering which is described in terms of Regge exchange. Such models can incorporate scaling by inserting appropriate residue functions into the Regge description.

Theoretical models [19,20,21] have related the behavior of νW_2 in the neighbourhood of $\omega \simeq 1$ to the elastic form factor at large q^2. If the elastic form factor $G(q^2) \to (1/q^2)^{\frac{n}{2}}$ as $q^2 \to 0$, then the predicted behavior for νW_2 is $\nu W_2 \to (1 - \frac{1}{\omega})^{n-1}$ as $\omega \to 1$. For either ω or $\omega' < 2$ the experimental values of νW_2 can be satisfactorily fit with a single cubic term, a result which is consistent with this prediction.

It is of interest to examine the explicit q^2 dependence of W_2 at constant W in the scaling region. Since for $\omega > 4$, which corresponds to $\frac{W^2 - M^2}{q^2} > 3$, the quantity νW_2 is approximately constant, we find that

$$W_2 \propto \frac{1}{1 + q^2/(W^2 - M^2)}$$

which is a relatively weak dependence on q^2. For $1 \leq \omega \leq 2$, νW_2 is proportional to $(1 - 1/\omega)^3$ and the dependence of νW_2 is

$$W_2 \propto \left[\frac{1}{W^2 - M^2 + q^2}\right] \left[\frac{W^2 - M^2}{q^2}\right]^3.$$

It is thus evident that for $\frac{W^2 - M^2}{q^2} << 1$, W_2 has the same q^2 dependence as the elastic form factor squared. The q^2 dependence is clearly intermediate between these extremes for intermediate values of ω.

Several sum rules based on current algebra and the use of current commutators have been proposed for inelastic electron scattering. Gottfried[22] has calculated a constant-q^2 sum rule based on a non-relativistic point-like quark model of the proton which is:

$$\int_1^\infty \frac{d\omega}{\omega} (\nu W_2) = 1$$

where the integral includes the contribution from the elastic cross-section. Using $R = 0.18$, interpolations of both the small and large angle data were used to determine νW_2 at a constant value of $q^2 = 1.5$ GeV^2. The evaluation of the integral when integrated over the range of the data gives

$$\int_1^{20} \frac{d\omega}{\omega} \nu W_2 = 0.78 \pm 0.04$$

This integral can be shown in a parton model to be equal to the sum of the squares of the charges of the constituents. Since the experimental values of νW_2 at large ω do not exclude a constant value for νW_2 there is some suspicion that this sum might diverge. This would imply that in the quark model the scattering has to occur from an infinite sea of quark-anti-quark pairs as well as from the valence quarks. The experimental value for the

Callan-Gross[23] sum $\int_1^\infty \frac{d\omega}{\omega^2} \nu W_2$, which is related to the equal time commutator of the current and its time derivative, is 0.172 $\pm$ .009 for an upper limit of the integral of $\omega = 20$. Unlike the previous sum, the value of this integral is not very sensitive to the behavior of νW_2 above $\omega = 20$. This integral is also important in parton theories [16] where its value is the mean square charge per parton. The experimental value is about one half the value predicted on the basis of the simple three quark model of the proton, and it is also too small for a proton described by a quark model with three valence quarks in a sea of quark-anti-quarks. However, a model[17] which includes neutral gluons in addition to the valence quarks and the sea of quark-anti-quark pairs is compatible with the experimental result.

Recently, Bloom and Gilman [21] have proposed a constant q^2 finite energy sum rule based on scaling in ω' that equates an integral over νW_2 in the resonance region with the corresponding integral over the asymptotic expression for νW_2. They have pointed out that the applicability of the sum rule to spectra which have prominent resonances is indicative of a substantial non-diffractive component in νW_2. The sum rule requires that J_1 equal J_2 with

$$J_1 \equiv \left(\frac{2M_p}{q^2}\right) \int_0^{\nu_m} d\nu \; (\nu W_2)_{exp}$$

and $$J_2 \equiv \left(\frac{2M_p}{q^2}\right) \int_0^{\nu_m} d\nu \; F(\omega') = \int_1^{\omega'_m} d\omega' \; F(\omega')$$

where $(\nu W_2)_{exp}$ is given by interpolation, at fixed q^2, of the 6^o and 10^o data with $R = 0.18$ and where $F(\omega')$ is a parametric representation of the

experimental values of νW_2 for $W > 1.8$ GeV and $q^2 > 1$ GeV^2. The upper limit is determined by choosing a missing mass W_m which is somewhat beyond the prominent resonance bumps and $2M\nu_m = W_m^2 - M_p^2 + q^2$. We find that in the range of q^2 from 1 to $4(\frac{GeV}{c})^2$ and W_m from 2.2 to 2.5 GeV the maximum deviation of J_2 from J_1 is 9%. This result is only weakly sensitive to modest changes in R.

The behavior of the inelastic cross-section has interesting implications with regard to the properties of the total absorption cross-sections for virtual photons, σ_t and σ_s. As has been discussed, σ_t is dominant in the scaling region. On the basis of the parton model, this is what one would expect if the constituents of the proton were spin 1/2 objects. Figure 11 shows the cross-sections σ_t and σ_s plotted for constant q^2 as functions of W^2. The dashed lines indicate the W^2 dependence of $\sigma_{\gamma p}$, which is the limit of $\sigma_t(q^2, \nu)$ as $q^2 \to 0$. For $q^2 \leq 3$ GeV^2 the cross-sections are consistent with a constant or a slowly falling energy dependence similar to the behavior of $\sigma_{\gamma p}$. For larger q^2, σ_t shows a rising energy dependence resembling a threshold type behavior. This rising behavior of σ_t at high energy is unique among the various total cross-sections that have been measured. The q^2 dependence of σ_t, shown in Figure 12, shows no pure power law behavior but varies in the region of the present data between $1/q^2$ and $1/q^6$ as indicated by the straight lines shown in Figure 12. The point $\omega' = 5$ roughly separates the threshold region of νW_2 from the flat, structureless region. The rising energy dependence of σ_t for large q^2 reflects the rising behavior of νW_2 for $\omega' < 5$. The $1/q^2$ dependence is correlated with the constancy of νW_2 for $\omega' > 5$, and the $1/q^6$ asymptotic dependence as ω' approaches unity corresponds to the asymptotic limit of the threshold behavior of νW_2.

$$\lim_{\substack{q^2 \to \infty \\ W^2 \text{constant}}} \nu W_2 = \frac{K}{4\pi^2\alpha}(\sigma_t + \sigma_s) \propto \lim_{\substack{q^2 \to \infty \\ W^2 \text{constant}}} \left(\frac{1}{1 + \frac{q^2}{W^2}}\right)^3 \propto \frac{1}{q^6}$$

A series of measurements of inelastic scattering from deuterium has recently been carried out covering the same kinematic regions as the previous work on the proton but with some extension to higher incident energies and lower scattered energies. Measurements of scattering from the proton were simultaneously made in order to reduce possible systematic errors in a comparison of the scattering from the two targets. The purpose of the deuterium studies was to extract the cross-section for inelastic scattering from the neutron. A comparison of neutron and proton cross-sections is a sensitive probe of the presence of a non-diffractive component in the scattering process, since a difference in the two would reveal the existence of some isotopic spin exchange. Measurements also were made of scattering from Be, Al, Cu, and Au, in order to test the A dependence of the inelastic scattering. I will report only some preliminary results from the deuterium-proton comparisons at 6^o and 10^o, as the other data are not sufficiently analysed for presentation.

On the basis of the impulse approximation, scattering from the deuteron is regarded as the sum of scattering from the neutron and the proton; however, a number of corrections have to be considered. Corrections have to be made in a deuteron-proton comparison for the internal motion in the deuteron. Other effects are the Glauber correction which is estimated to be less than a percent, the effect of mesonic currents in the deuteron which is assumed to be small from the information derived from elastic electron-deuteron scattering, and the effect of the final state interaction which cannot be estimated but is assumed to be small. In the following discussion the quantity D-H, the

deuterium cross-section minus the hydrogen cross-section,will be assumed to represent the neutron cross-section. An estimate of the "smearing correction" due to the internal motion will be shown. Values of (D/H) - 1 , which represent with the above limitations values of the neutron cross-section divided by the proton cross-section, are plotted against ω in Figure 13. The points shown represent data having values of $q^2>1$ GeV^2 and W > 2 GeV. These results indicate sizeable differences between the neutron and proton cross-sections and thus provide evidence for a significant non-diffractive component in the scattering process. The values of the ratio are consistent with a single function of ω and so within the errors the neutron cross-section exhibits scaling. With the expected reduction in the presently shown errors from further data analysis and with the inclusion of deuterium data from the large angle measurements a more stringent test for scaling behavior of the neutron will soon be available.

Corrections for internal motion have been studied by West[24] who included effects due to the requirement of gauge invariance in the interaction with the deuteron. An independent investigation using somewhat different approximations has been carried out by the MIT experimental group[25]. The results of the two approaches are in reasonably good agreement. It was found that the sensitivity of the correction on various deuteron wave functions was small, provided that the wave function was consistent with the observed electromagnetic form factor of the deuteron. The variation in the correction for these wave functions was less than a few percent. Figure 14 shows the effect of the smearing correction as calculated by the MIT group on the plot of (D/H) - 1 versus ω. The dashed curve represents a curve drawn through the uncorrected points shown in Figure 13. The solid curve represents the dashed curve after smearing corrections have been made. The vertical lines represent

the band of errors in the experimental curve. The "smearing" effects for the points shown are thus smaller than the errors in the experimental points and cannot account for the differences between the neutron and proton observed in Figure 13. The corrected curve shown in Figure 14 is actually the ratio of the neutron to proton cross-sections with both including the effects of internal motion. Rather than take internal motion effects out of the neutron cross-section they were inserted into proton cross-section, which is a good deal simpler to do. A computational program is now underway to remove the effects of the internal motion from the deuteron data. The value of the corrected curve at a given value of ω is thus the ratio of neutron to proton cross-sections averaged over a small region of ω around the given value. Figure 15 represents $\left[2 - (D/H)\right] \nu W_{2p}$ uncorrected for smearing, as a function of ω. On the assumption that the values of R for neutron and proton are equal this plot represents $\nu W_{2p} - \nu W_{2n}$. There is a suggestion of a maximum of this quantity at about $\omega \simeq 3$. With these results, the constant q^2 inequality of Bjorken [26] can be tested.

$$\int_1^\infty \frac{d\omega}{\omega} \left[\nu W_{2p} + \nu W_{2n}\right] \gtrsim 1/2$$

This inequality appears to be satisfied for $\omega \gtrsim 5$.

Before concluding this talk, I would like to discuss some of the recent inelastic muon scattering results from SLAC[27]. A 12 GeV/c muon beam was scattered from hydrogen, carbon, and copper targets. Measurements of inelastic scattering were made for $0.3 \lesssim q^2 \lesssim 2(\text{GeV/c})^2$ and $0.6 \lesssim \nu \lesssim 6$ GeV. In order to extract the ratio of neutron to proton cross-sections data were analysed in kinematic regions where possible shadowing effects due to a ρ

dominance mechanism would be minimized. In these regions, the minimum momentum transfer for ρ production $t_{min} = \frac{(q^2 + M_\rho^2)^2}{4\nu^2}$ was large. With this requirement the A dependence found was $A^{0.99 \pm .01}$, showing that there was no detectable shadowing. This data yielded an average ratio of neutron to proton cross-section of $0.91 \pm .06$. Since the range of ω for this data is $\omega > 5$ the electron and muon scattering results are consistent. The muon scattering group has made a detailed study [28] of the comparison of the muon and electron scattering results in the regions of kinematic overlap. Figure 16 shows a comparison of the results. The agreement is excellent. Since the radiative corrections for muon scattering are about a factor of four smaller than for electron scattering, this comparison confirms the conclusion that the radiative corrections are not introducing an appreciable error into the electron scattering results. I would like to stray off the general topic of this talk to discuss one further conclusion arising from this comparison. The muon scattering group has used these results to put a limit on any possible difference in interaction between the muon and the electron. Using the conventional form for a breakdown parameter $\frac{1}{\Lambda_d^2} = \frac{1}{\Lambda_\mu^2} - \frac{1}{\Lambda_e^2}$, they find that $\Lambda_d > 4.1$ GeV at a 98% confidence level for data with $q^2 < 4.0(\text{GeV/c})^2$ and $\nu < 9$ GeV.

This is all that I have time to discuss today. In the next few months there should be many new results coming from the ongoing analysis of recent SLAC-MIT experiments and from continuing experiments[29] studying the production of secondaries in deep inelastic electron scattering.

FIGURE CAPTIONS

1. The radiatively corrected spectrum measured at $\theta = 6^{\circ}$, E = 7 GeV. The elastic peak and the radiative tail from the elastic scattering have been subtracted.
2. The radiatively corrected spectrum measured at $\theta = 6^{\circ}$, E = 16 GeV. The elastic peak and the radiative tail from elastic scattering have been subtracted.
3. Effects of the radiative corrections:
   a. uncorrected spectrum
   b. corrected spectrum
   c. ratio of corrected to uncorrected spectrum.

   $\frac{d^2\sigma}{d\Omega dE'}$, is shown as a function of the missing mass of the final hadronic state.
4. Sketches of the behavior of radiatively corrected e-p cross-sections for various incident energies.
5. Sketches of the behavior of radiatively corrected e-p cross-sections for various scattering angles. The 1.5 degree curve is taken from other SLAC-MIT data used to obtain total photo-absorption cross-sections.
6. Measured values of $R = \sigma_s/\sigma_t$ as a function of q^2 for various values of W. Also shown are the predictions from the ρ meson dominance model calculated for W = 3.5 GeV.
7. The quantity νW_2 versus q^2 for $\omega = 4$ and $W > 2$ GeV.
8. The quantity νW_2 for various ranges of ω plotted against q^2. νW_2 is kinematically constrained to zero for $q^2 = 0$. Preliminary results. Possible systematic errors are not included in the errors shown. R is assumed constant and equal to 0.18.

Figure Captions, continued

9. $2M_pW_1$ and νW_2 are shown as functions of ω for R = 0.18, W > 2.6 GeV and $q^2 > 1$ GeV^2.

10. $2M_pW_1$ and νW_2 are shown as functions of ω' for R = 0.18 and W > 1.80 GeV and $q^2 > 1$ GeV^2.

11. Values of σ_t and σ_s are shown at constant q^2 as a function of W^2 (or ν) for q^2 = 1.5, 3, 5, and 8 GeV^2. Also shown is the ν dependence of the total photoabsorption cross-section.

12. Values of σ_t are shown at constant W as a function of q^2 for W = 2, 2.5 and 3.0 GeV. The solid line indicates a $1/q^2$ dependence and the dashed line represents a $1/q^6$ variation with q^2. The point ω' = 5 is also indicated.

13. The quantity (D/H)-1 plotted against ω. The corrections for the effects due to the internal motion of the nucleons in the deuteron are shown in Figure 14. The Glauber correction is negligible. On the assumption that the final state interaction and scattering from meson currents are small, the ordinate should approximate the ratio of neutron to proton scattering cross-sections.

14. The effect of the correction for internal motion on the plot of (D/H) - 1. The dashed curve represents a curve drawn through the uncorrected points as shown in Figure 13. The solid curve represents the dashed curve after corrections have been made. The vertical lines represent the band of errors in the experimental curve. The smearing effects do not account for the observed differences between the neutron and proton cross-sections.

15. The quantity $(\nu W_{2p} - \nu W_{2n})$ as a function of ω derived from the points in Figure 13 with the assumption that $R_n = R_p$.

Figure Captions, continued

16. Comparisons of cross-sections for μ-p and e-p scattering. The values of ρ are the ratios of the μ-p to e-p cross sections; the quantity $K = \frac{W^2 - M^2}{2M}$.

TABLE I

Range of Kinematics of SLAC-MIT Inelastic Data

Spectra were measured for the following scattering angles and incident energies:

Angle θ		Incident Energy E (GeV)	Range of q^2 $(GeV/c)^2$
6°	20 GeV Spectrometer	19.5, 16.0, 13.5, 10.0, 7.0, 4.5	3.5 - 0.3
10°		19.3, 17.7, 15.2, 13.5, 11.0, 9.0, 7.0, 4.9	8.9 - 0.6
18°	20 GeV Spectrometer	17.0, 13.3, 10.4, 8.6, 6.5, 4.5	14.0 - 1.0
26°		18.0, 15.0, 11.9, 8.6, 6.7, 4.5	20 - 1.5
34°		15.0, 12.5, 10.0, 7.9, 5.8, 4.5	17 - 2.0

REFERENCES

1. The people who have participated in the SLAC-MIT work presented here are:

   E.D. Bloom, M. Breidenbach, G. Buschhorn, R.L. Cottrell, D.H. Coward, H. De Staebler, W.R. Ditzler, J. Drees, J.I. Friedman, G.C. Hartmann, C.L. Jordan, H.W. Kendall, G. Miller, L.W. Mo, H. Piel, J.S. Poucher, R.E. Taylor.

2. W. Bartel, B. Dudelzak, H. Krehbiel, J. McElroy, U. Meyer-Berkhout, W. Schmidt, V. Walther, and G. Weber, DESY Report 68/53 (1968); W. Albrecht, F.W. Brasse, H. Dorner, W. Flanger, K. Frank, E. Gaussage, J. Gayler, H. Hultschig, and J. May, DESY Report 69/7 (1969).

3. M.L. Perl, T. Braunstein, J. Cox, F. Martin, W.T. Toner, B.D. Dieterle, T.F. Zipf, W.L. Lakin, and H.C. Bryant, Phys. Rev. Letters 23 1191 (1969).

4. More experimental details are given in: E.D. Bloom, et al., Phys. Rev. Letters 23 935 (1969) and SLAC-PUB 815 (to be published in the Physical Review).

5. The data for the 4.89 GeV curve in Figure 4 are taken from reference 2 (DESY Report 68/53) with the addition of crude radiative corrections. The top curve in Figure 5 is from SLAC scattering data at $\theta_{lab} = 1.5^{\circ}$ (to be published). These data were taken to obtain the total γ_p cross-section.

6. S.D. Drell and J.D. Walecka, Ann. Phys. (N.Y.) 28, 18 (1964).

7. L.N. Hand, Phys. Rev. 129, 1834 (1963).

8. J.J. Sakurai, Phys. Rev. Letters 22, 981 (1969).

9. E.D. Bloom, D.H. Coward, H. DeStaebler, G. Miller, L.W. Mo, and R.E. Taylor; and M. Breidenbach, J.I. Friedman, G.C. Hartmann, and H.W. Kendall, Phys. Rev. Letters 23, 930 (1969); also Phys. Rev. Letters 23, 935 (1969).

10. J.D. Bjorken, Phys. Rev. 179, 1547 (1969).

11. E.D. Bloom, et al., Report presented to the XV International Conference on High Energy Physics, Kiev, USSR, (September, 1970). This report is available as SLAC-PUB-796.

12. Ashok suri, Phys. Rev, Letters, 26 208 (1971).

13. V. Rittenberg and H.R. Rubinstein, Phys. Letters 35B, 50 (1971).

14. J.I. Friedman, H.W. Kendall; and E.D. Bloom, D.H. Coward, H. DeStaebler, J. Drees, C.L. Jordan, G. Miller, R.E. Taylor, SLAC-PUB-907; also SLAC-PUB 815; to be published in Phys. Rev.

15. R.P. Feynman (unpublished); also, Phys. Rev. Letters 23 1415 (1969), and

References, continued

Proceedings of the Third Topical Conference on High Energy Collisions of Hadrons, Stony Brook 1969.

16. J.D. Bjorken and E.A. Paschos, Phys. Rev. 185 1975 (1969).

17. J. Kuti, and V.F. Weisskopf, MIT-CTP Pub. 211 (1971), submitted to Phys. Rev.

18. J.W. Moffat and V.G. Snell Phys, Rev. 3D, 2848 (1971).

19. S. Drell and T.M. Yan, Phys. Rev. Letters 24 181 (1970).

20. G. West, Phys. Rev. Letters 24, 1206 (1970).

21. F.D. Bloom and F.J. Gilman, Phys. Rev. Letters 25 1140 (1970).

22. K. Gottfried, Phys. Rev. Letters 18, 1174 (1967).

23. C.G. Callan, Jr. and D.J. Gross, PHys. Rev. Letters 21, 311 (1968).

24. G. West, (to be published).

25. M. Sogard, A. Bodek, J.I. Friedman (unpublished).

26. J.D. Bjorken, Phys. Rev. Letters 16, 408 (1966).

27. W.L. Lakin, T.J. Braunstein, J. Cox, B.D. Dieterle , M.L. Perl, W.T. Toner, T.F. Zipf, and H.C. Bryant, Phys. Rev. Letters 26, 34 (1971).

28. W.T. Toner, et al., SLAC-PUB-868; submitted for publication in Phys. Rev. Letters

29. D.E. Andrews, K. Berkelman, D.G. Cassel, D.L. Hartill, J. Hartmann, R. Kerchner, E. Lazarus, R.M. Littauer, R.L. Loveless, R. Rohlfs, D.H. White, A.J. Sadoff, Phys. Rev. Letters 26 864 (1971); F.W. Brasse, W. Fehrenbach, W. Flauger, K.H. Frank, J. Gayler, V. Korbel, J. May, and P.D. Zimmermann and E. Gaussauge, DESY 71/79; K. Heinloth, DESY (Private Communication); R.E. Taylor, SLAC (Private Communication).

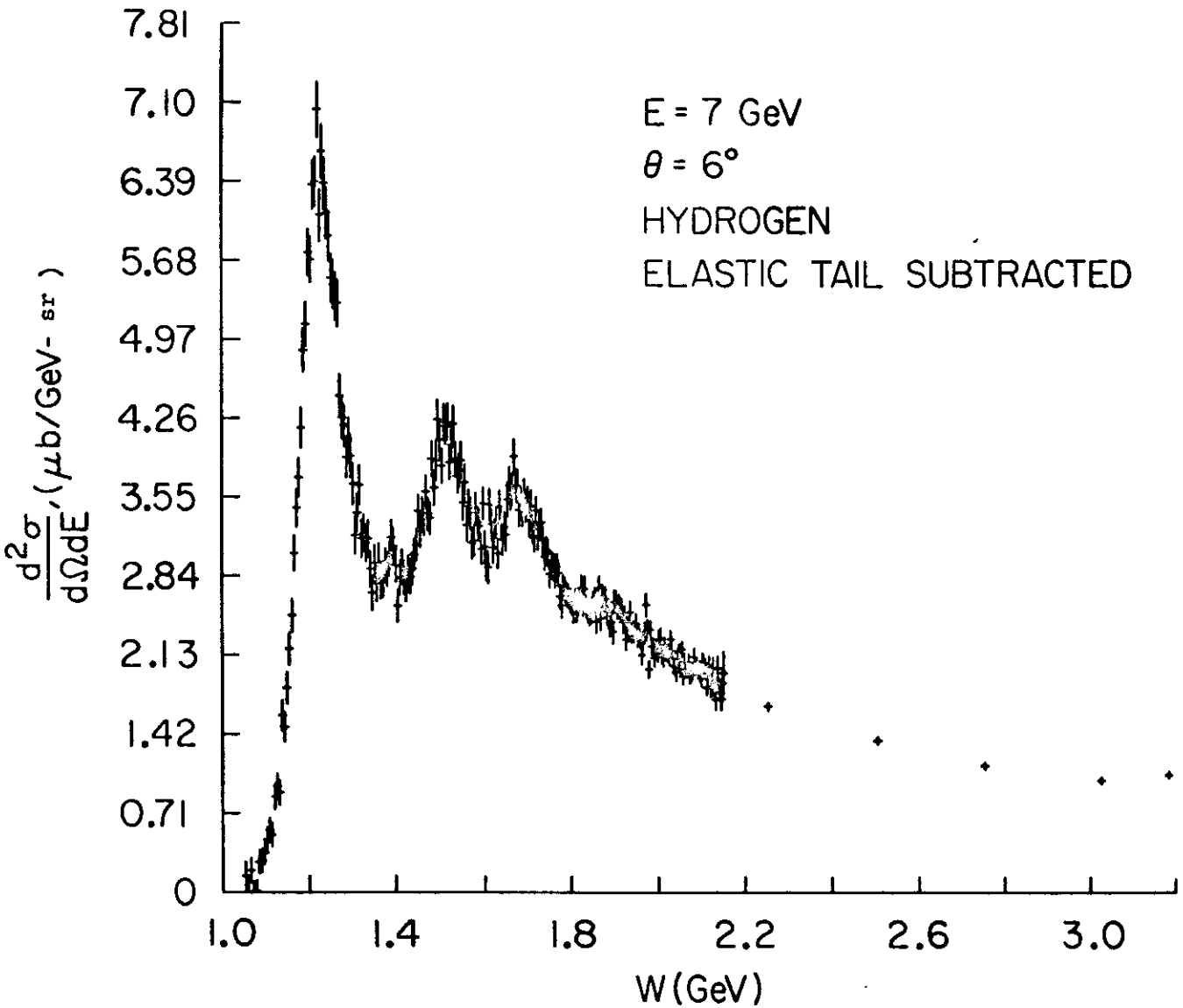
7.81
7.10
6.39
5.68
4.97
4.26
3.55
2.84
2.13
1.42
0.71
0
1.0
1.4
1.8
2.2
2.6
3.0
W(GeV)
$\frac{d^2\sigma}{d\Omega dE'}$, ($\mu$b/GeV-sr)
E = 7 GeV
θ = 6°
HYDROGEN
ELASTIC TAIL SUBTRACTED

Fig. 1

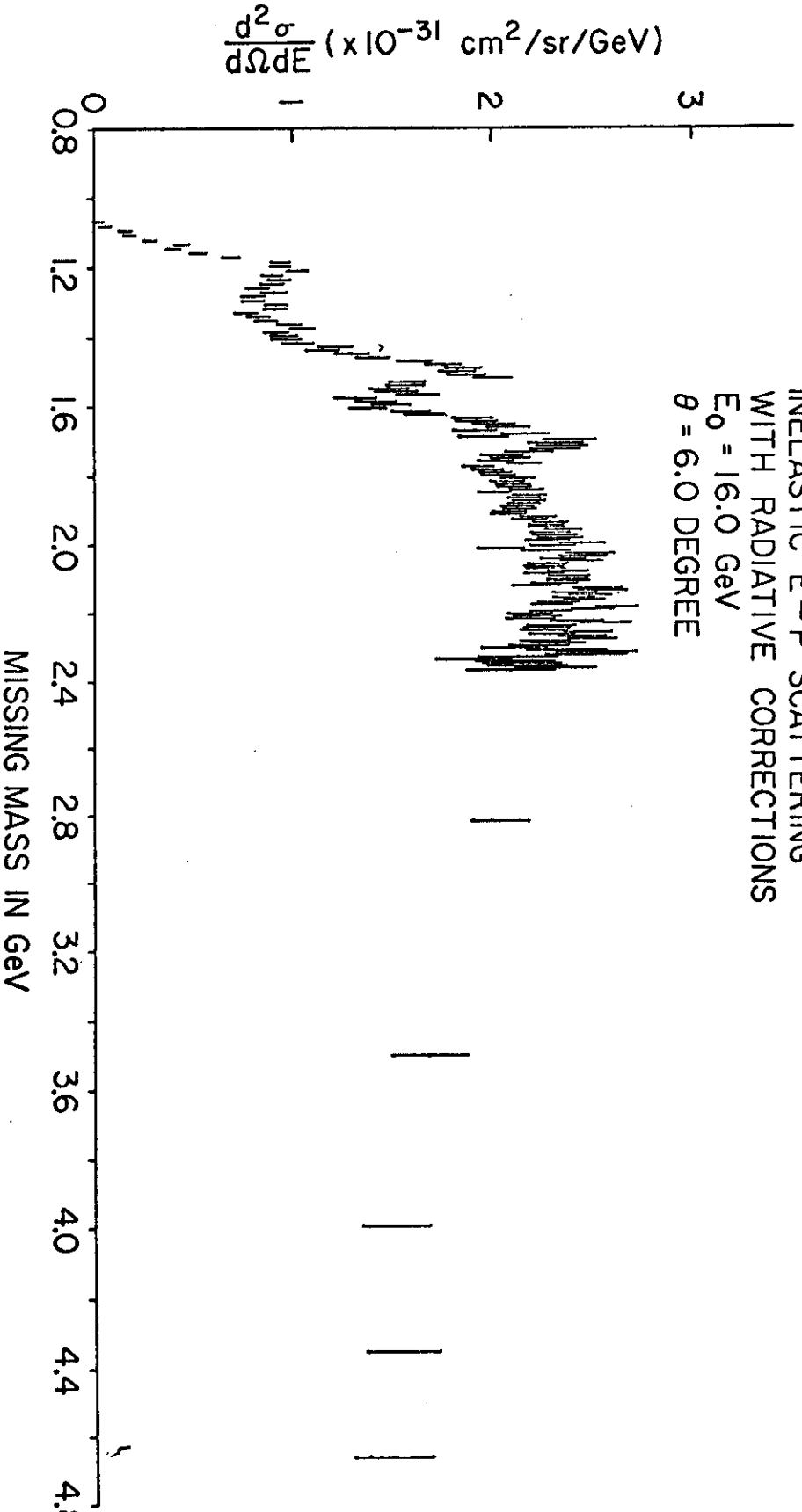
$\frac{d^2\sigma}{d\Omega dE}$ (x 10^{-31} cm^2/sr/GeV)
0
1
2
3
INELASTIC E-P SCATTERING
WITH RADIATIVE CORRECTIONS
E_o = 16.0 GeV
θ = 6.0 DEGREE
0.8
1.2
1.6
2.0
2.4
2.8
3.2
3.6
4.0
4.4
4.8
MISSING MASS IN GeV

Fig. 2

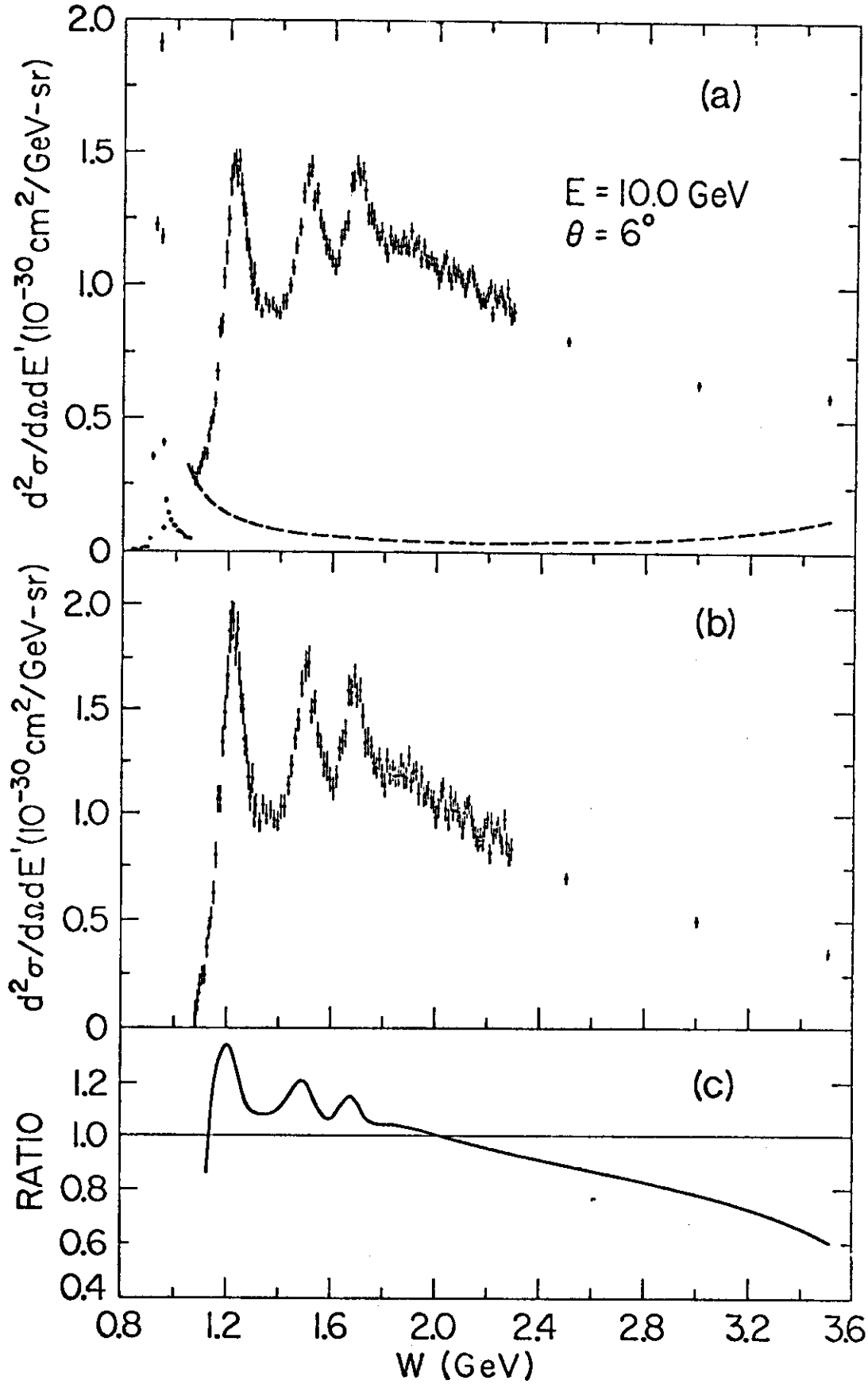
(a)
E = 10.0 GeV
θ = 6°
(b)
(c)
$d^2\sigma/d\Omega dE'(10^{-30}cm^2/GeV\text{-}sr)$
RATIO
W (GeV)
0
0.5
1.0
1.5
2.0
0.4
0.6
0.8
1.2
0.8
1.2
1.6
2.0
2.4
2.8
3.2
3.6

Fig. 3

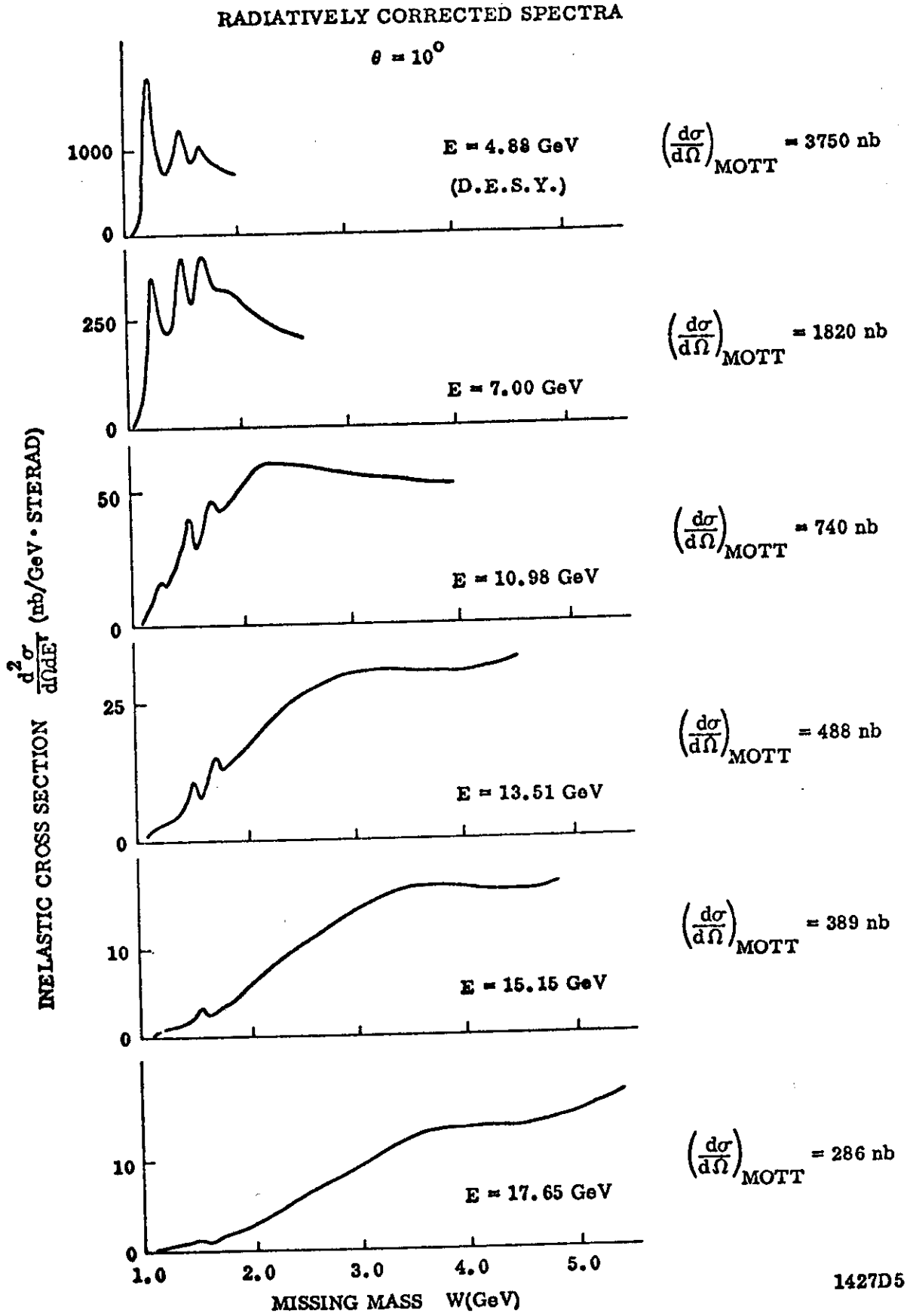
RADIATIVELY CORRECTED SPECTRA
θ = 10°
E = 4.88 GeV
(D.E.S.Y.)
(dσ/dΩ)MOTT = 3750 nb
E = 7.00 GeV
(dσ/dΩ)MOTT = 1820 nb
E = 10.98 GeV
(dσ/dΩ)MOTT = 740 nb
E = 13.51 GeV
(dσ/dΩ)MOTT = 488 nb
E = 15.15 GeV
(dσ/dΩ)MOTT = 389 nb
E = 17.65 GeV
(dσ/dΩ)MOTT = 286 nb
1000
250
50
25
10
10
0
1.0
2.0
3.0
4.0
5.0
INELASTIC CROSS SECTION d²σ/dΩdE' (nb/GeV • STERAD)
MISSING MASS W(GeV)
1427D5

Fig. 4

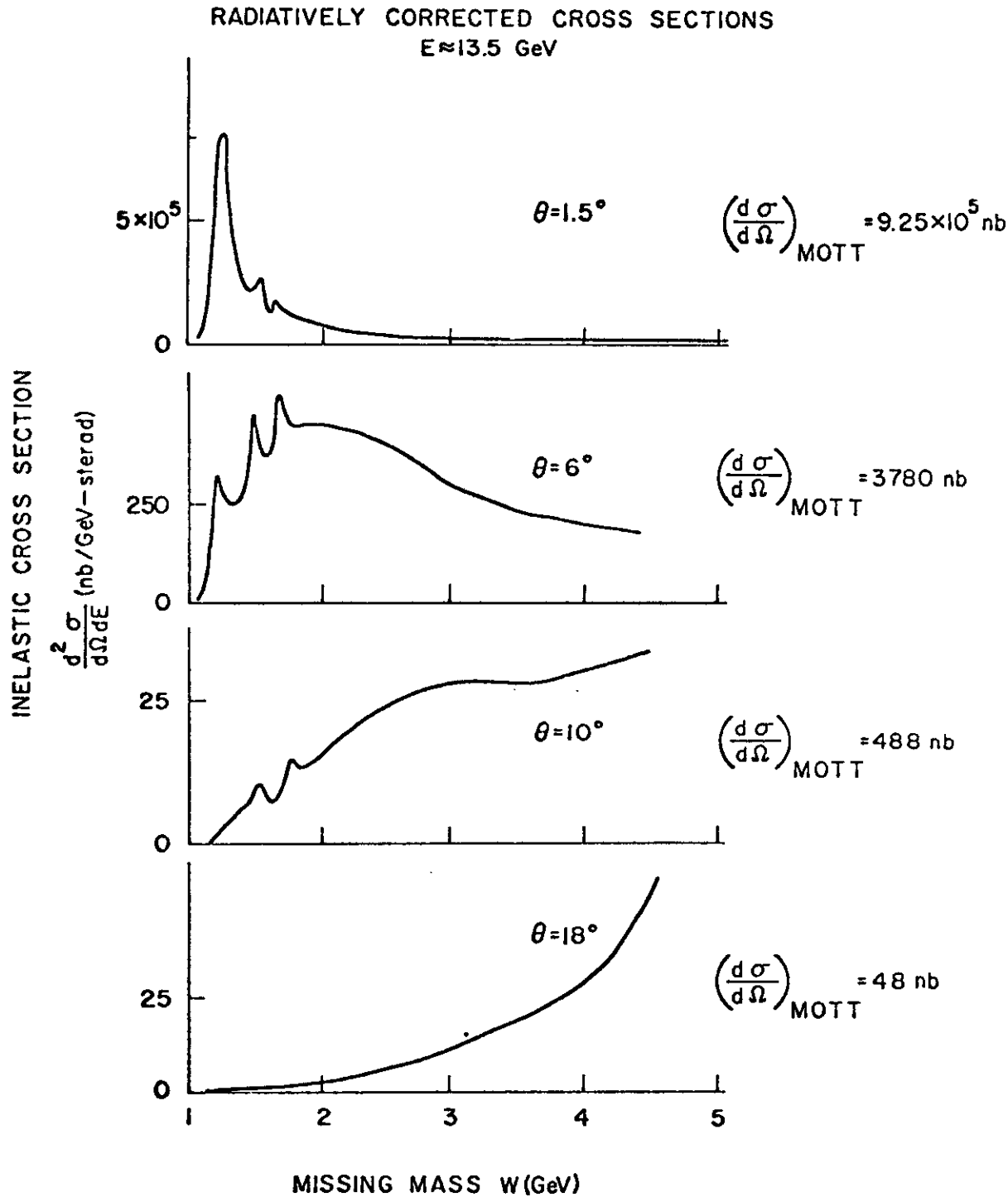
RADIATIVELY CORRECTED CROSS SECTIONS
E≈13.5 GeV
INELASTIC CROSS SECTION
$\frac{d^2\sigma}{d\Omega dE}$ (nb/GeV-sterad)
5×10^5
0
θ=1.5°
$\left(\frac{d\sigma}{d\Omega}\right)_{MOTT}$ =9.25×10^5 nb
250
0
θ=6°
$\left(\frac{d\sigma}{d\Omega}\right)_{MOTT}$ =3780 nb
25
0
θ=10°
$\left(\frac{d\sigma}{d\Omega}\right)_{MOTT}$ =488 nb
25
0
θ=18°
$\left(\frac{d\sigma}{d\Omega}\right)_{MOTT}$ =48 nb
1
2
3
4
5
MISSING MASS W(GeV)

Fig. 5

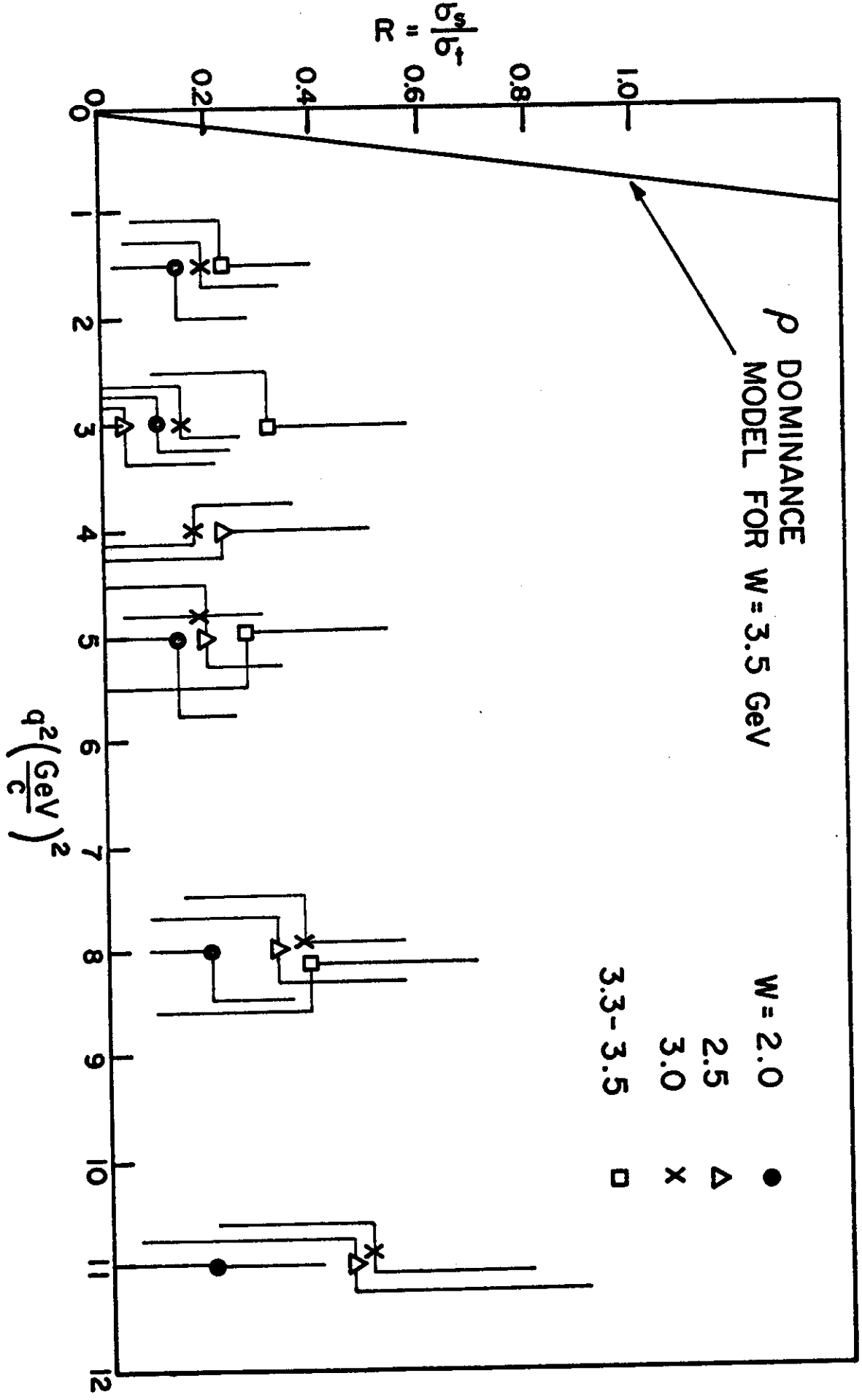
$R = \frac{\sigma_s}{\sigma_t}$
0.0
0.2
0.4
0.6
0.8
1.0
$q^2\left(\frac{GeV}{c}\right)^2$
0
1
2
3
4
5
6
7
8
9
10
11
12
ρ DOMINANCE MODEL FOR W = 3.5 GeV
W = 2.0 ●
2.5 △
3.0 ×
3.3-3.5 □

Fig. 6

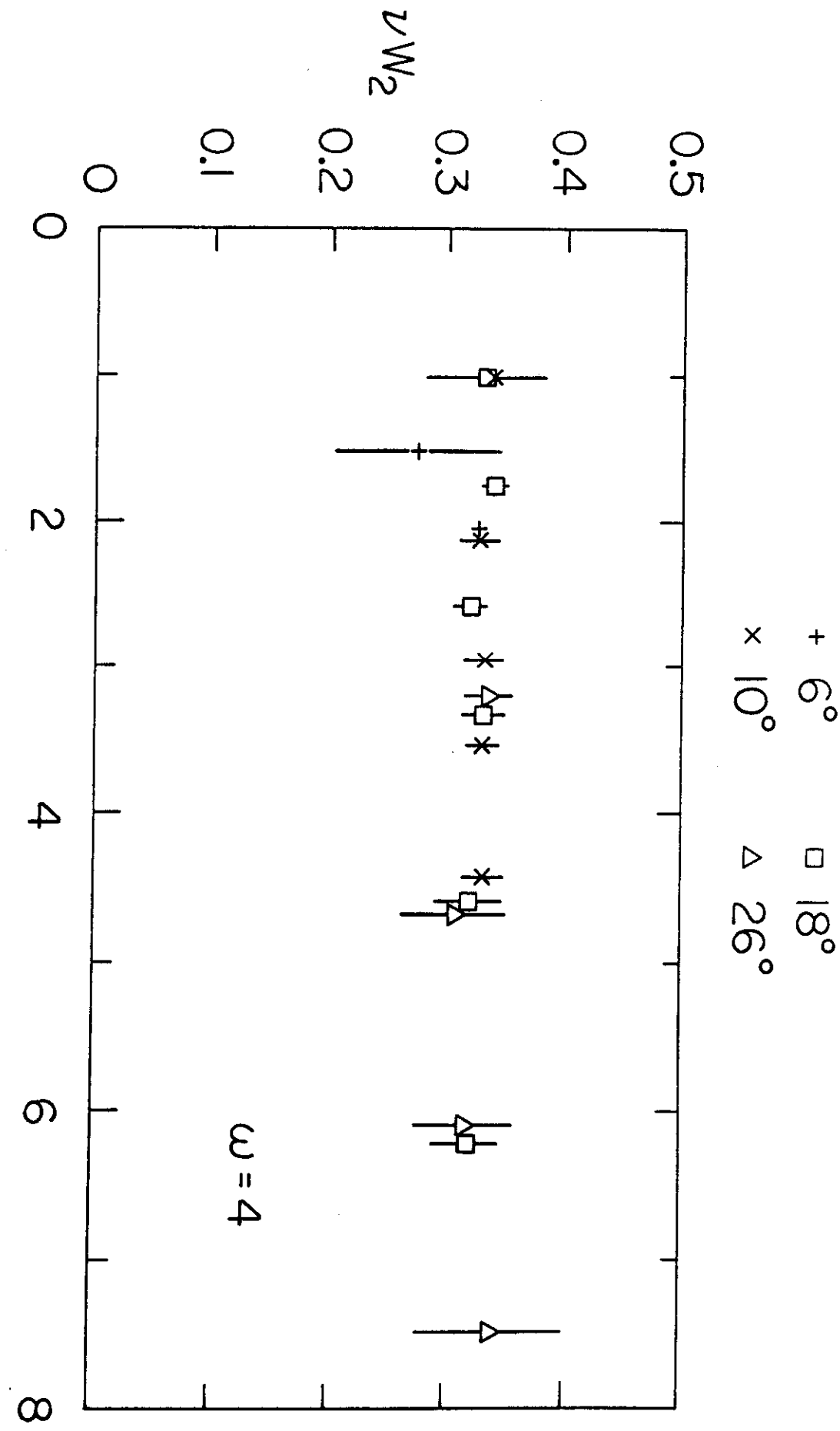

Fig. 7

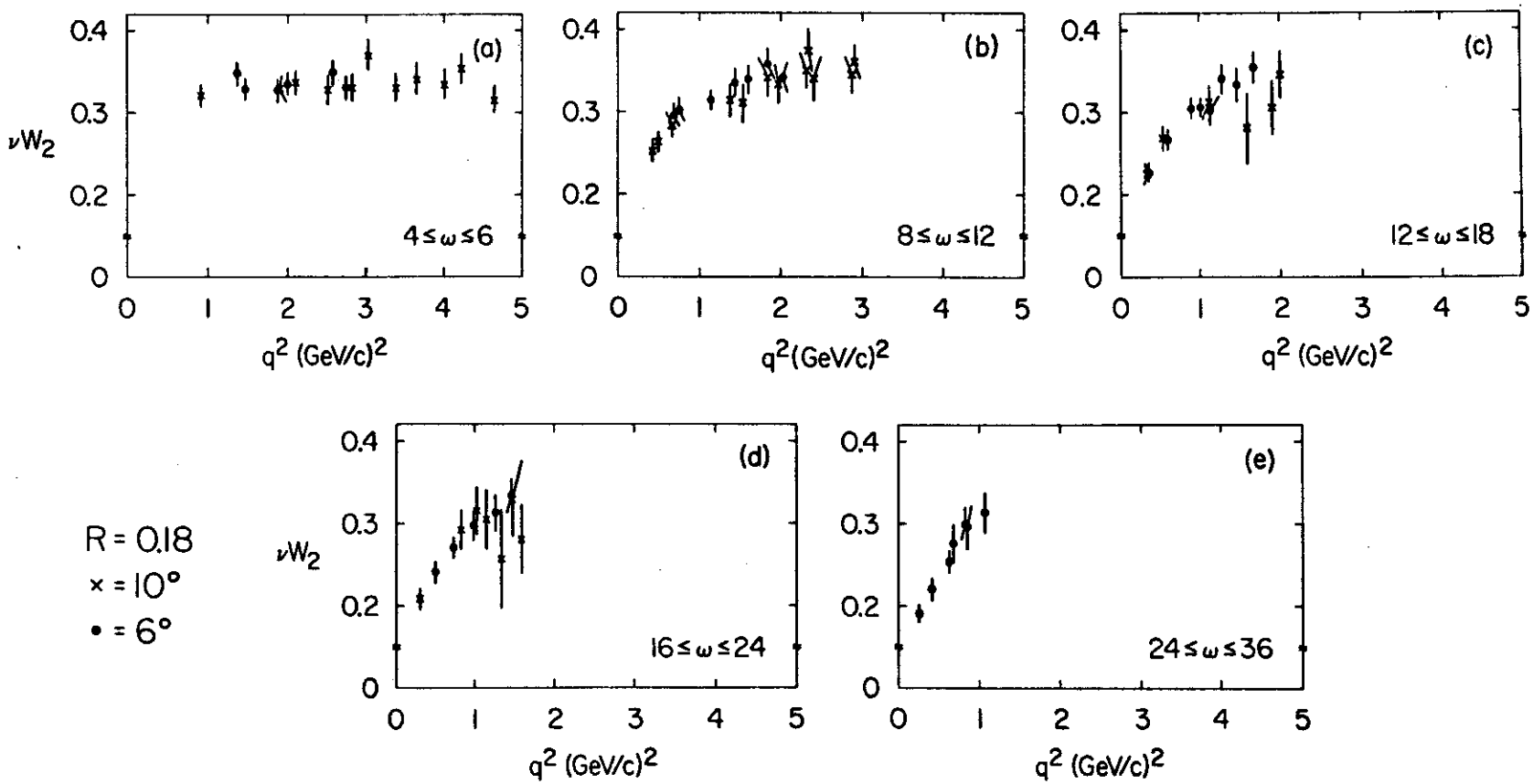

Fig. 8

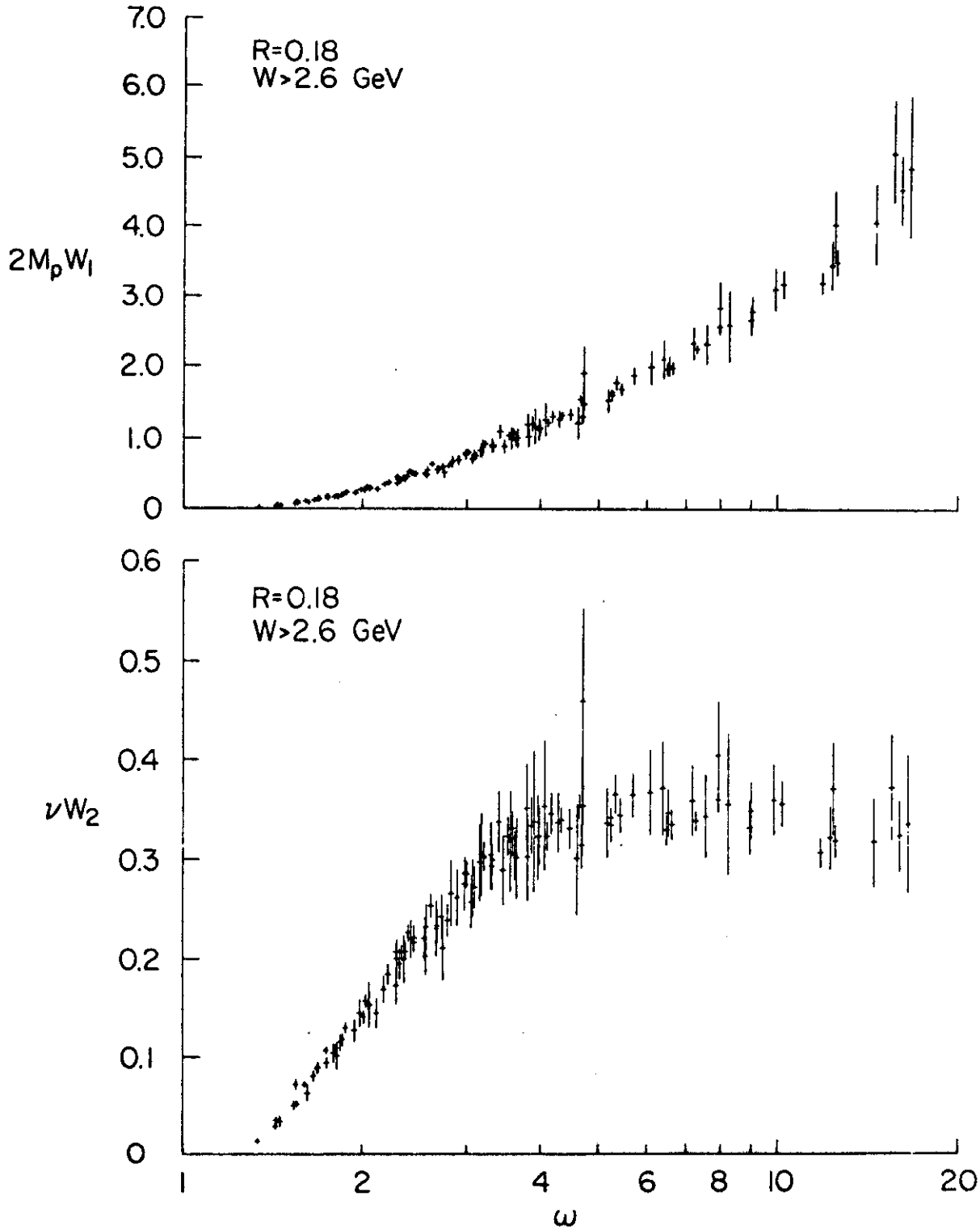
7.0
6.0
5.0
4.0
3.0
2.0
1.0
0
$2M_pW_1$
R=0.18
W>2.6 GeV
0.6
0.5
0.4
0.3
0.2
0.1
0
νW_2
R=0.18
W>2.6 GeV
1
2
4
6
8
10
20
ω

Fig. 9

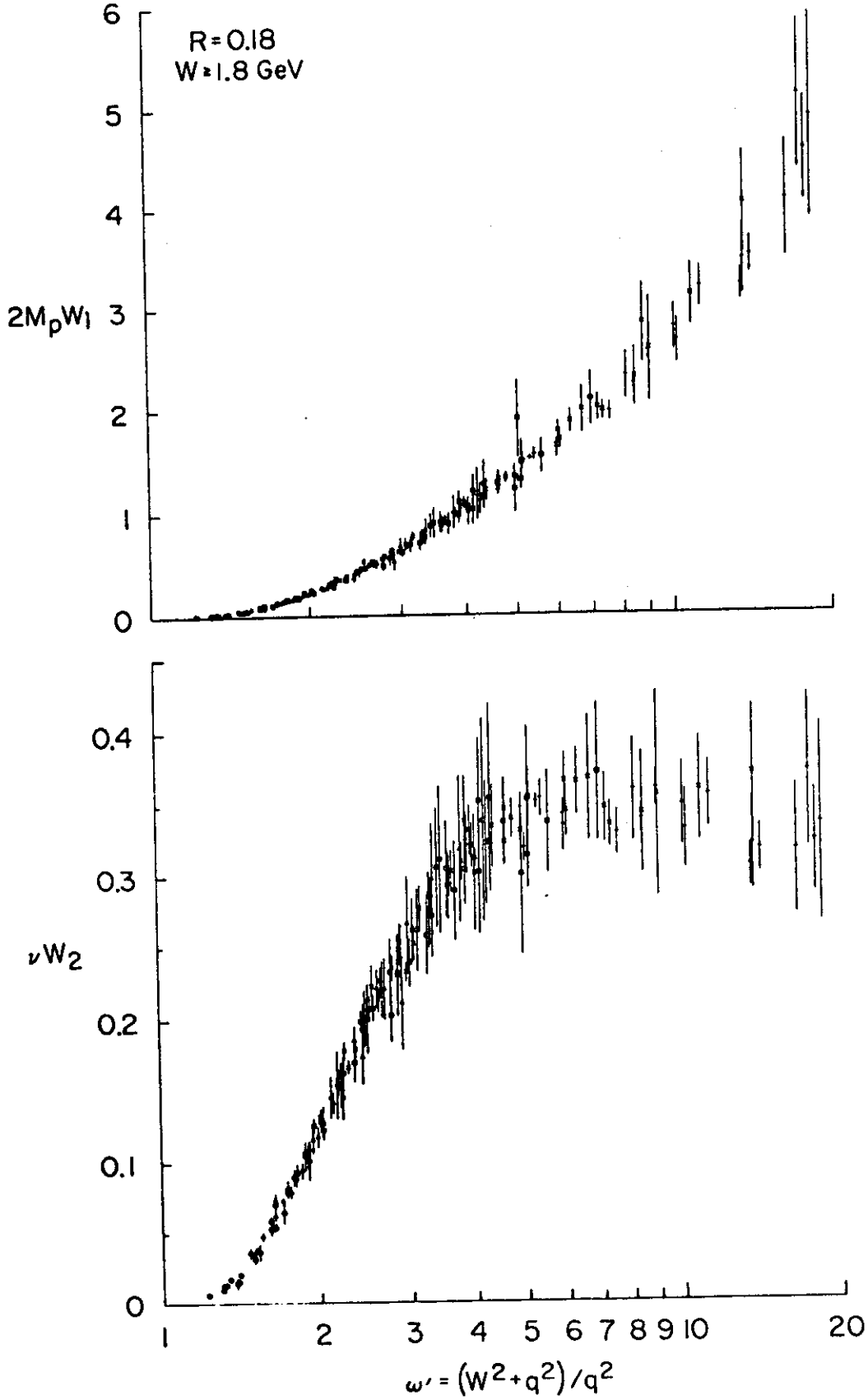
R = 0.18
W ≥ 1.8 GeV
$2M_pW_1$
νW_2
$\omega' = (W^2+q^2)/q^2$
0
1
2
3
4
5
6
0.1
0.2
0.3
0.4
1
2
3
4
5
6
7
8
9
10
20

Fig. 10

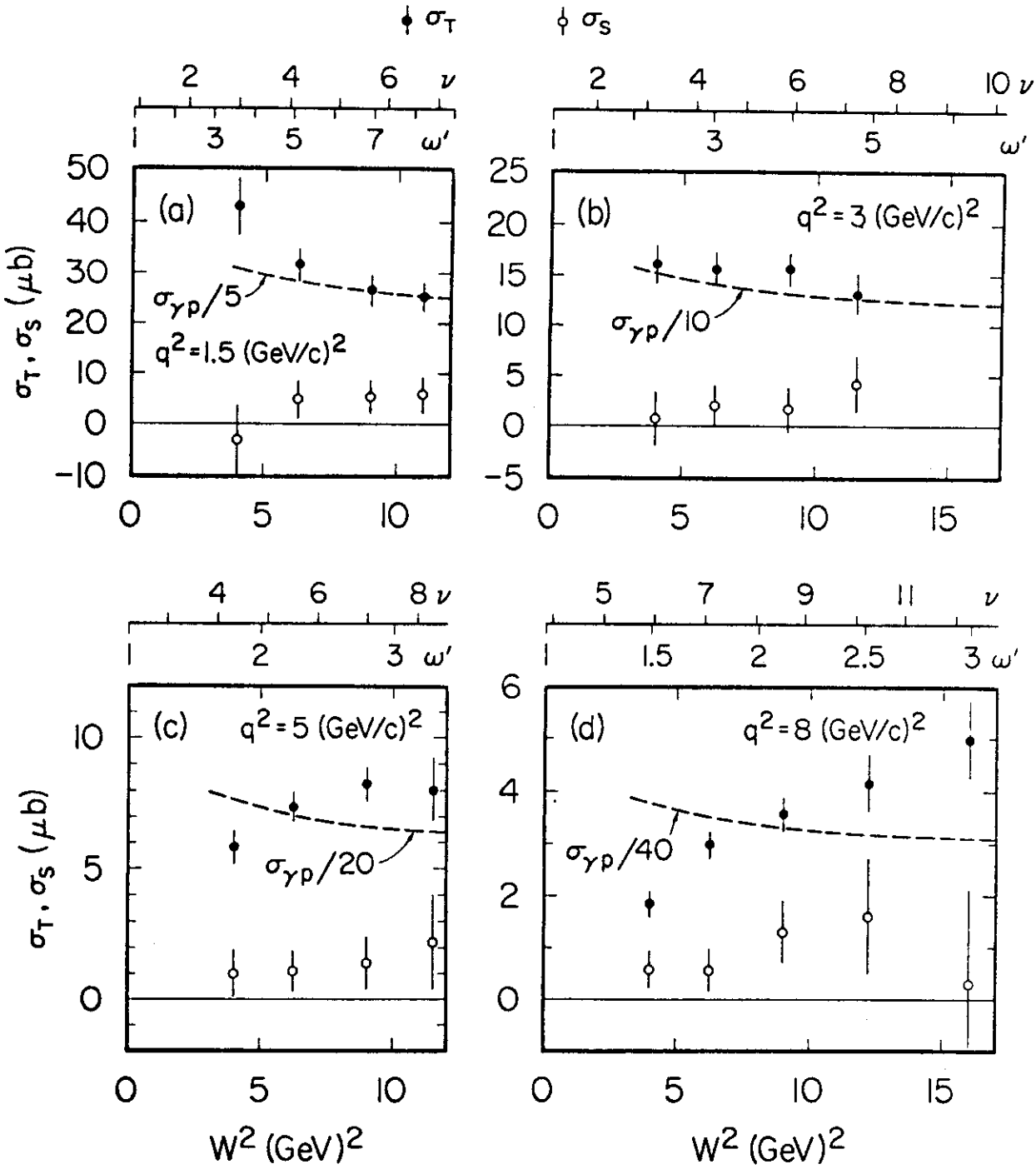
σT
σS
(a)
(b)
(c)
(d)
q2=1.5 (GeV/c)2
q2=3 (GeV/c)2
q2=5 (GeV/c)2
q2=8 (GeV/c)2
σγp/5
σγp/10
σγp/20
σγp/40
σT, σS (μb)
W2 (GeV)2
ν
ω'

Fig. 11

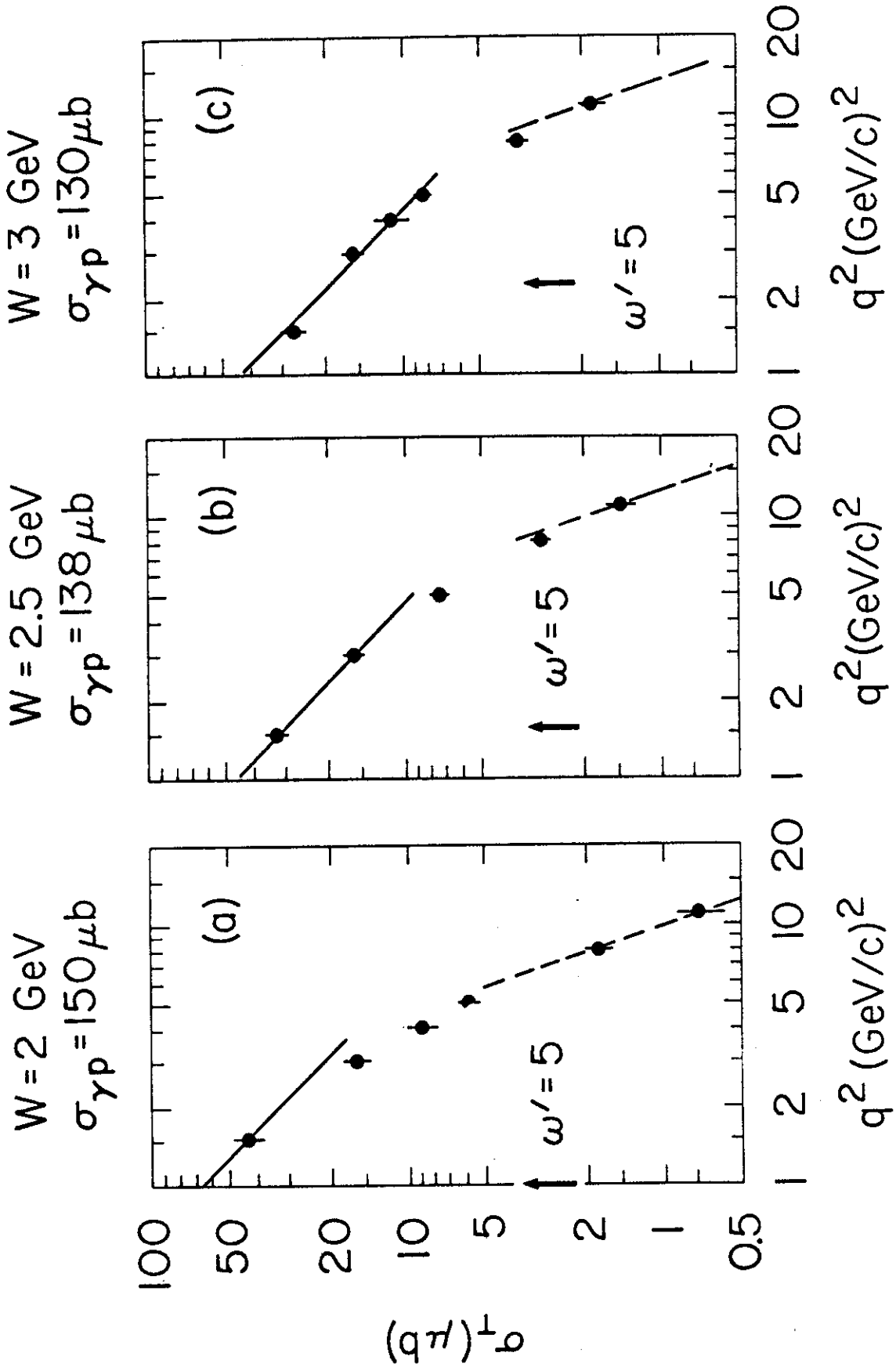
W = 2 GeV
$\sigma_{\gamma p}$ = 150 μb
(a)
ω′ = 5
W = 2.5 GeV
$\sigma_{\gamma p}$ = 138 μb
(b)
ω′ = 5
W = 3 GeV
$\sigma_{\gamma p}$ = 130 μb
(c)
ω′ = 5
σ_T(μb)
100
50
20
10
5
2
1
0.5
1
2
5
10
20
q^2 (GeV/c)^2

Fig. 12

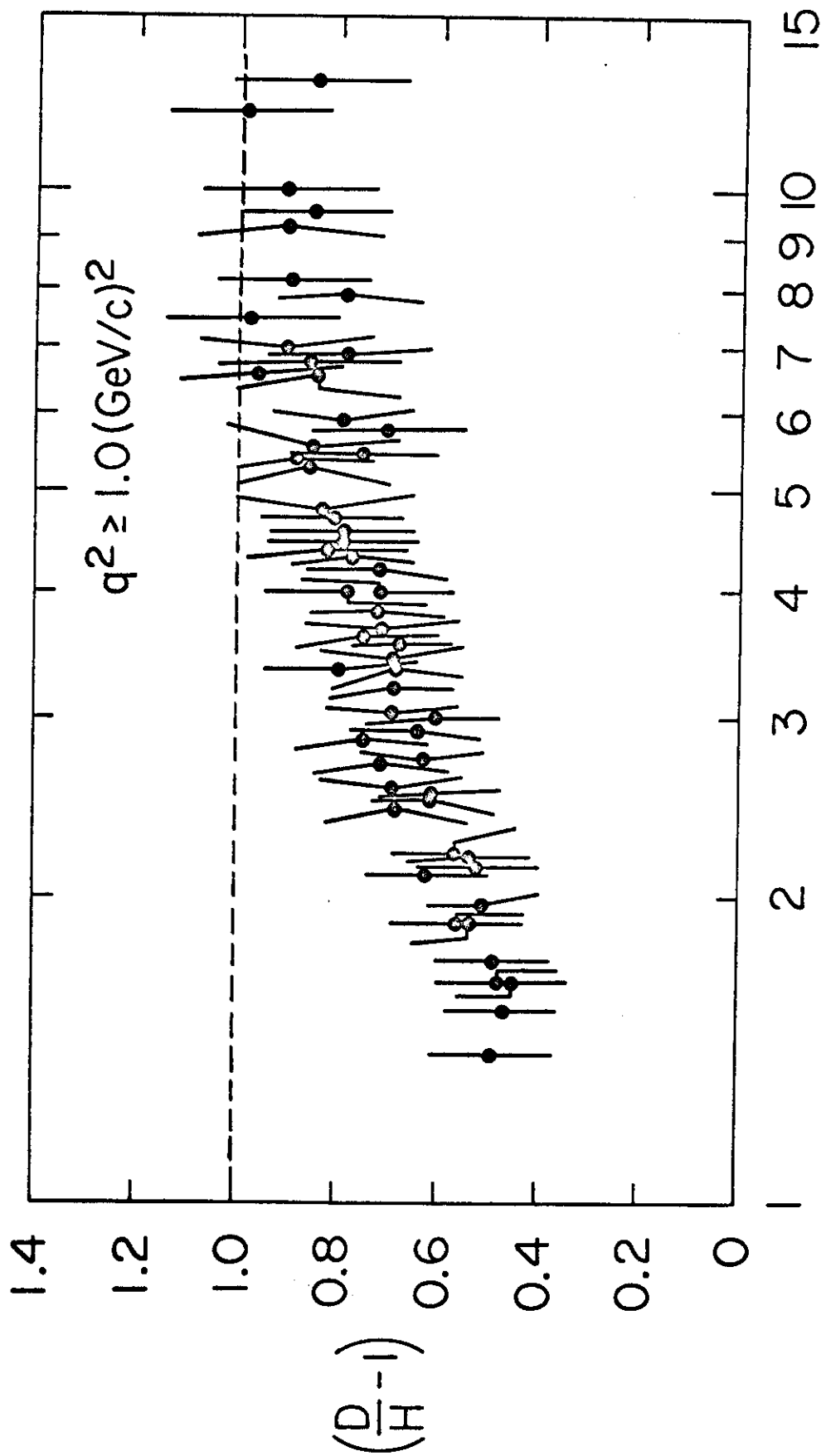
$q^2 \geq 1.0 (GeV/c)^2$
ω
$\left(\frac{D}{H}-1\right)$
1.4
1.2
1.0
0.8
0.6
0.4
0.2
0
1
2
3
4
5
6
7
8
9
10
15

Fig. 13

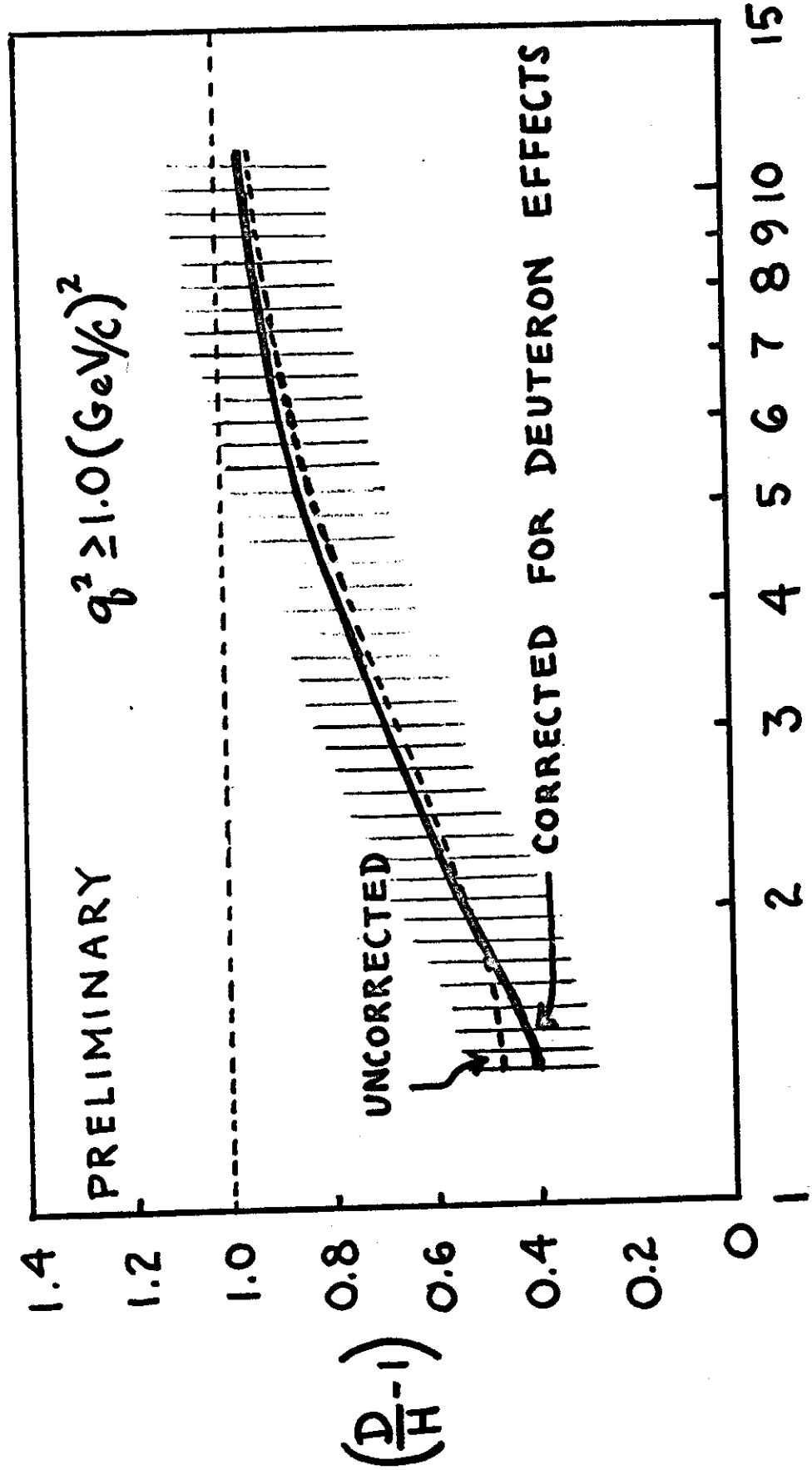
PRELIMINARY
$q^2 \geq 1.0 (GeV/c)^2$
UNCORRECTED
CORRECTED FOR DEUTERON EFFECTS
$\left(\frac{D}{H}-1\right)$
1.4
1.2
1.0
0.8
0.6
0.4
0.2
0
1
2
3
4
5
6
7
8
9
10
15
ω

Fig. 14

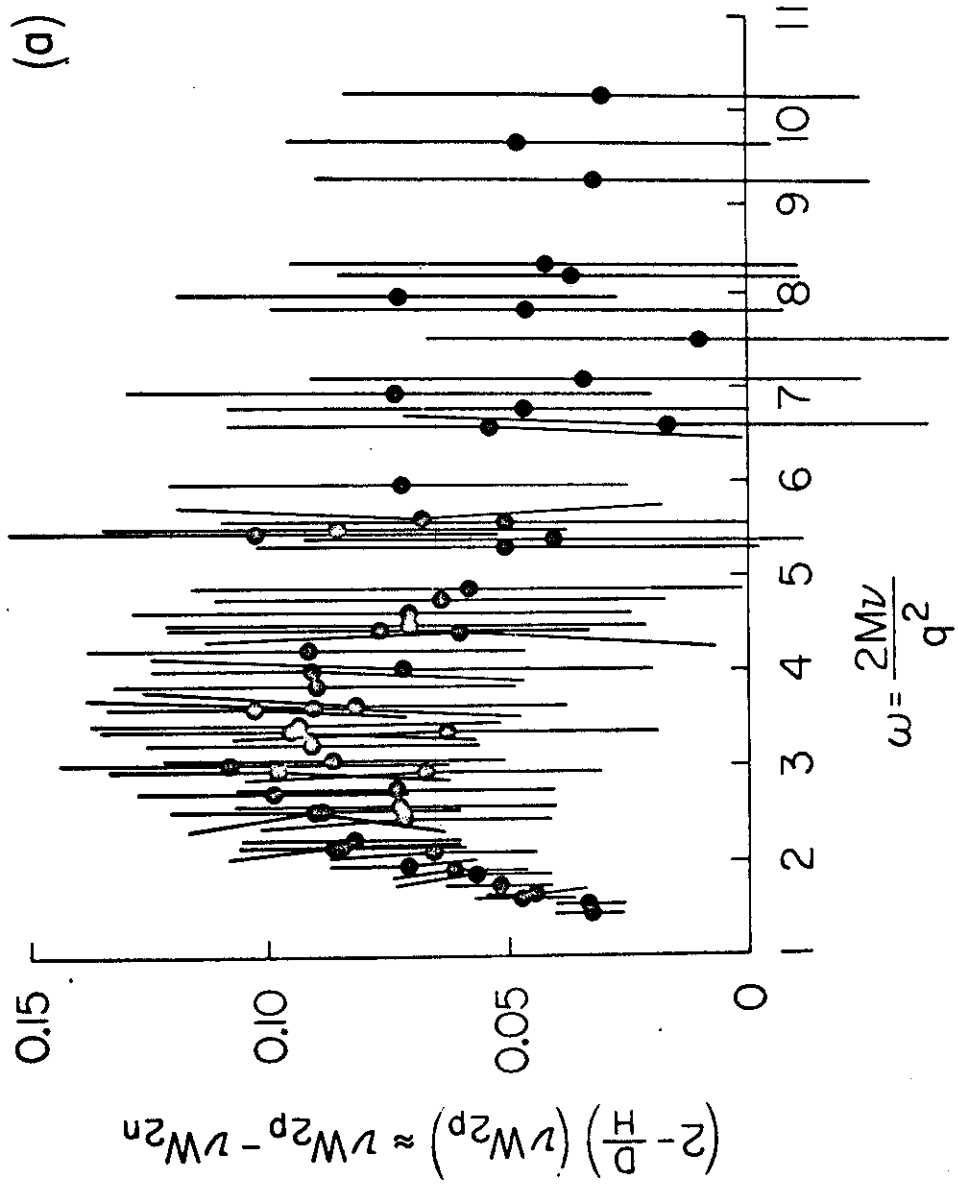
(a)
$(2-\frac{D}{H})(\nu W_{2p}) \approx \nu W_{2p} - \nu W_{2n}$
0.15
0.10
0.05
0
1
2
3
4
5
6
7
8
9
10
11
$\omega = \frac{2M\nu}{q^2}$

Fig. 15

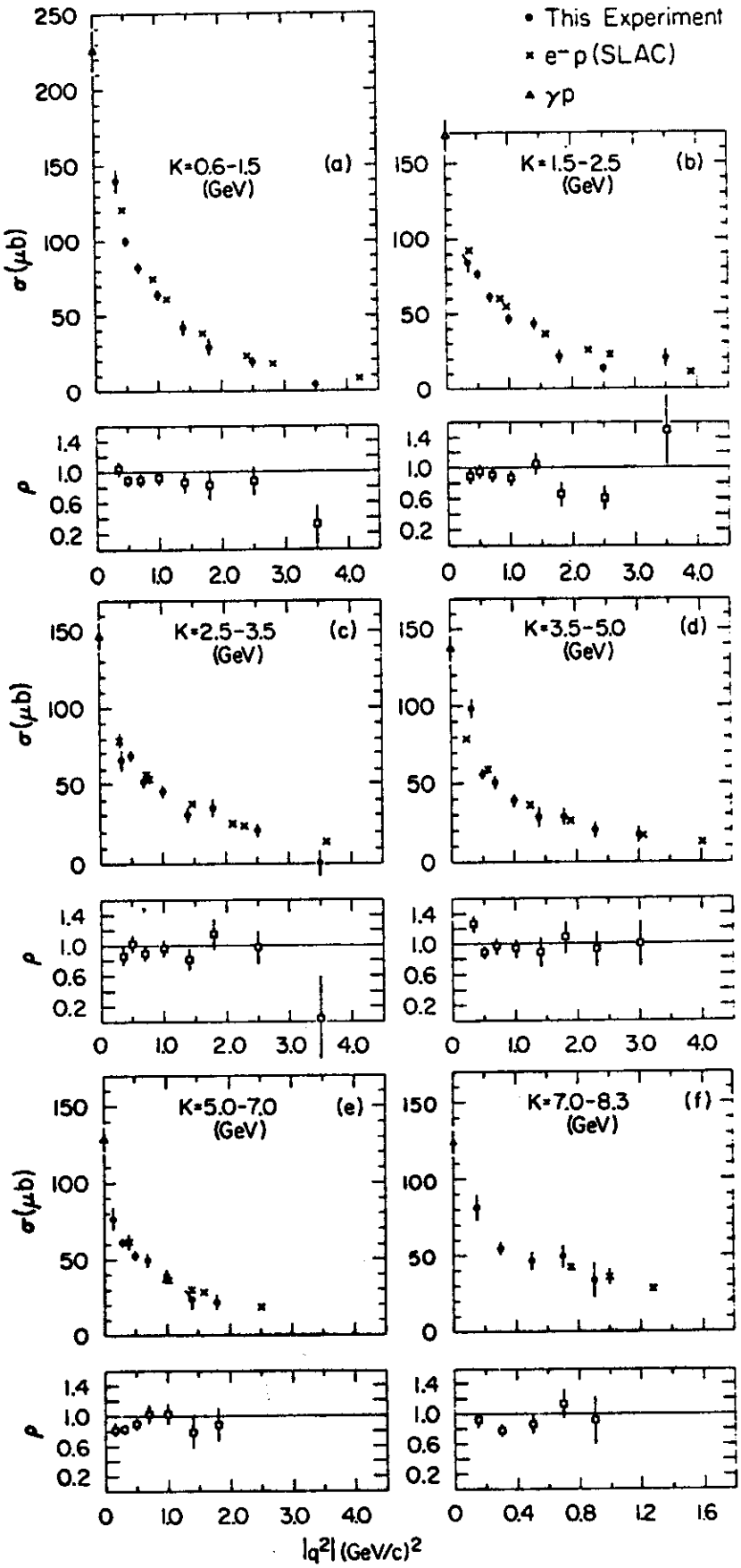
• This Experiment
× e⁻p (SLAC)
▲ γp
K=0.6-1.5 (GeV) (a)
K=1.5-2.5 (GeV) (b)
K=2.5-3.5 (GeV) (c)
K=3.5-5.0 (GeV) (d)
K=5.0-7.0 (GeV) (e)
K=7.0-8.3 (GeV) (f)
σ(μb)
ρ
|q²| (GeV/c)²

Fig. 16